Dissimilar anisotropy of electron versus hole bulk transport in anatase TiO_2: Implications for photocatalysis

Donghun Kim,[1] Byung Chul Yeo,[1,2] Dongbin Shin,[3] Heechae Choi,[1] Seungchul Kim,[1] Noejung Park,[3] and Sang Soo Han[1,*]

[1]*Computational Science Research Center, Korea Institute of Science and Technology, Seoul 02792, Korea*

[2]*School of Electrical and Electronic Engineering, Yonsei University, Seoul 03722, Korea*

[3]*Department of Physics, Ulsan National Institute of Science and Technology, Ulsan 44919, Korea*

(Received 17 May 2016; revised manuscript received 24 August 2016; published 19 January 2017)

Recent studies on crystal facet manipulation of anatase TiO_2 in photocatalysis have revealed that reduction and oxidation reactions preferably occur on (100)/(101) and (001) facets, respectively; however, a fundamental understanding of their origin is lacking. Here, as a result of first-principles calculations, we suggest that a *dissimilar* trend in the anisotropy of electron vs hole bulk transport in anatase TiO_2 can be a dominant underlying mechanism for the difference in photochemical activity. Photoexcited electrons and holes are driven to different facets, i.e., electrons on (100)/(101) and holes on (001), leading to the observed preference for either reduction or oxidation. This trend of electrons vs holes found in pure TiO_2 applies even for cases where a variety of dopants or defects is introduced.

DOI: 10.1103/PhysRevB.95.045209

I. INTRODUCTION

Photocatalysis (PC) has recently attracted a great deal of attentions as it provides a promising pathway for both clean energy (e.g., hydrogen fuel) production [1] and environmental sustainability [2]. Among many candidate semiconductor materials, TiO_2, the first prototype material for PC [3], is widely used today because of its advantages regarding desired band-edge positions, long-term photochemical stability, and nontoxicity [1,4]. Two polymorphs of TiO_2, i.e., rutile and anatase, are used industrially. Although both polymorphs have been analyzed in great detail [5–7] from the perspective of PC, anatase generally exhibits relatively higher photocatalytic activity than the other due to its favorable electronic properties [7–9]. In the present work, we are mainly interested in anatase TiO_2, and thus TiO_2 hereafter refers to *anatase* TiO_2 unless otherwise specified.

It has been widely accepted that three low-index facets, (100), (101), and (001), dominate the surfaces of TiO_2 particles [10]. It has long been questioned which facet is the most effective for photocatalytic activity. However, in a practical sample, the ratio of a specific facet can hardly be controllable, and thus direct comparison of the photocatalytic activity between different facets has remained challenging. In this regard, the work of Yang *et al.* [11] is greatly noteworthy: they, for the first time, demonstrated that morphological control was possible using hydrofluoric acid as a shape-controlling agent. This work enables a variety of particle shapes to be tested in PC and to be compared in terms of activities [12–17]. These experiments have led to the interesting consensus that reduction and oxidation reactions preferably occur on different facets, i.e., reductions on (100)/(101) and oxidations on (001), respectively; now, these results require a fundamental understanding of their origin.

There already exist several efforts to reveal this phenomenon on the basis of surface atomic structures [18] or band-edge energies [13,19,20]; however, these efforts are restricted to *surface* properties, probably because chemical reactions themselves occur at the surfaces of photocatalysts. Unfortunately, little attention is given to the step prior to the actual reactions, namely, *bulk* transport of photoexcited carriers, despite the fact that about 90% of photogenerated carriers are lost during this step [21]. In this article, considering the phenomenon from the viewpoint of bulk transport, we offer a novel explanation complementing existing explanations.

As it has been unclear whether the dominant carrier transport mechanism is bandlike or polaronic in anatase TiO_2, we carried out two largely different sets of *ab intio* density functional theory (DFT) calculations in this work. In Sec. III A, assuming that carriers in anatase TiO_2 prefer a free-carrier state, we focus on a carrier transport property, namely, the carrier's effective mass (m^*). We investigate the anisotropy of the electron (m_e^*) and hole (m_h^*) effective masses in TiO_2 and discover that the anisotropic behavior is the *opposite* between an electron and a hole. With a particular interest in directions perpendicular to dominant facets, we find that electrons can be transported toward the (100)/(101) facets up to 3.95 times faster than holes can ($m_e^*/m_h^* = 3.95$), whereas holes are driven to the (001) facet 3.8 times faster than electrons are ($m_e^*/m_h^* = 0.26$), resulting in the (100)/(101) and (001) facets exhibiting different reductive and oxidative natures. To unveil the origin of this interesting trend, we thoroughly analyze orbital hybridizations near the conduction- and valence-band (CB and VB) edges along selected k directions (i.e., [100] and [001]), where nearest-neighbor hybridizations between Ti $3d$ and O $2p$ orbitals dominate only in the [100] direction for the CB and act oppositely in the [001] for the VB. Because it is very likely that imperfections such as dopants or defects exist in a practical sample, we demonstrate that the above observations can further be expanded to TiO_2 with dopants or intrinsic defects. In Sec. III B, motivated by polaronic features in this material, we have expanded our study to cases where polaron hopping is the dominant transport mechanism. Our polaron model presents dissimilar anisotropic manners of electron versus hole bulk transport and still supports the preferred accumulations of electrons on the (100)/(101) facets and holes on the (001) facet.

*sangsoo@kist.re.kr

II. METHODS

DFT calculations were performed using the plane-wave basis VASP code [22] with an energy cutoff of 400 eV and fast-Fourier-transform grid spacing of 0.2 Å in each lattice direction. The projector-augmented-wave method was adopted to describe the potential from the ionic core [23]. For Ti, $3p$ (semicore), $3d$, and $4s$ states were treated as valence states ($3p^6 4s^2 3d^2$ scheme). Integrations over the Brillouin zone were performed using a Monkhorst-Pack k-point sampling of $8 \times 8 \times 4$ after convergence tests. The geometry is fully relaxed until the maximum Hellmann-Feynman forces are less than 0.01 eVÅ^{-1} [24]. The hybrid functional of Heyd, Scuseria, and Ernzerhof (HSE06) is used [25]. In order to match the Kohn-Sham gap with the known one (3.2 eV), 20% of the exchange energy is substituted with the Hartree-Fock exact exchange.

It is important to note that we adopted different computational methods for polaron studies. We carried out spin-polarized DFT + U calculations using the generalized gradient approximation (GGA) of Perdew-Burke-Ernzerhof for the exchange correlation functional. We used a $3 \times 3 \times 2$ supercell to make the simulation cell sufficiently large (216 atoms) to accommodate lattice relaxations. Integrations over the Brillouin zone were performed using a Monkhorst-Pack k-point sampling of $4 \times 4 \times 2$. (This sampling is sufficiently dense for the supercells.) The geometry is fully relaxed using the conjugate gradient scheme until force components on every atom are less than 0.01 eVÅ^{-1}. Since standard DFT favors electron delocalization, polaron formation is not likely to happen. There are two well-known approaches to overcome this issue and successfully describe polaronic distortions within DFT formalism: (i) exact exchange is introduced to some extent in the exchange functional (i.e., hybrid functional), and (ii) the on-site Hubbard U term is added. As our supercells with 216 atoms are just too large to be tested in the hybrid functional scheme, the other approach (i.e., DFT + U), is selected in the present study. U parameters are given to Ti $3d$ for the extra electron case and to O $2p$ for the extra hole case, respectively. After extensive tests to find appropriate U parameters, we conclude that, for both the extra electron and the extra hole cases, the U value of 5 eV is the most suitable and, thus, is selected (see the Supplemental Material [46]).

III. RESULTS AND DISCUSSION

A. Anisotropy of bandlike transport in TiO_2

The TiO_2 in anatase polymorph can be described by four Ti and eight O atoms in a tetragonal unit cell, as shown in Fig. 1(a). The calculated lattice parameters ($a = 3.77$ Å and $c = 9.44$ Å) are in a good agreement with the experimentally measured values [26]. We and a previous theoretical work [8] have identified the nature of the indirect band gap. As shown in Fig. 1(b), one can observe that the CB minimum (CBM) occurs at the Γ point, whereas the VB maximum (VBM) occurs at $k = [\delta\delta 0]$ ($\delta \approx 0.44$). It is important to examine orbitals forming the edges of the CB and VB since the E-k dispersion is highly dependent on orbital hybridizations. As shown in the orbital-resolved projected density of states (PDOS) in

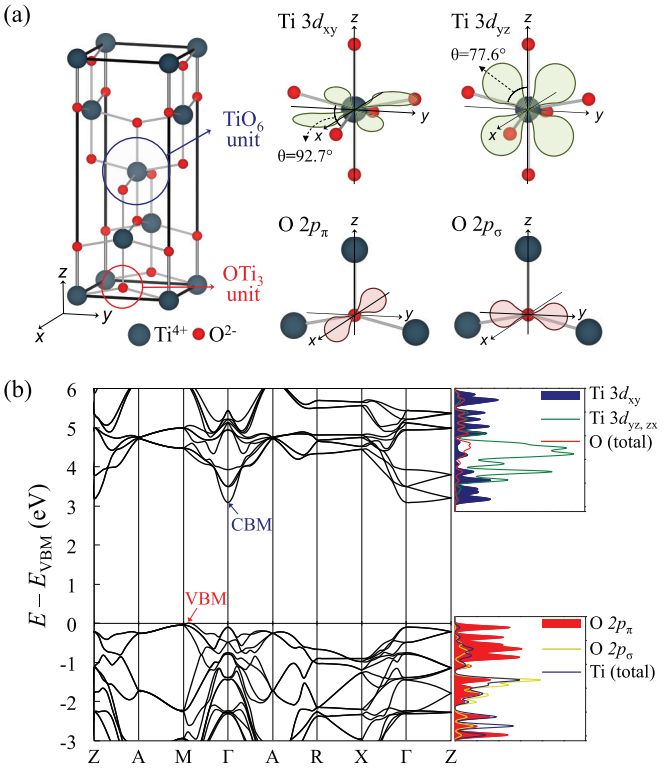

FIG. 1. Crystal and energy-band structures of TiO_2. (a) Unit cell of TiO_2. Blue and red circles signify a Ti-centered octahedronlike TiO_6 unit and an O-centered T-shape-like OTi_3 unit, with selected orbitals (Ti $3d_{xy,yz}$, O $2p_{\pi,\sigma}$) drawn at the right. (b) Calculated energy band structures along high-symmetry k directions. Orbital-resolved PDOSs are aligned at the right.

Fig. 1(b), the lowest CB primarily consists of Ti $3d$ orbitals, while the highest VB is predominantly contributed by O $2p$ [8,27]. In solids, however, the crystal field splits the degenerate free-ion levels. On the CB side, Ti t_{2g} ($3d_{xy,yz,zx}$) states, which are degenerate in a "perfect" octahedral environment, are now split due to Jahn-Teller structural distortions: they are broken into the single low-lying $3d_{xy}$ state and the twofold high-lying $3d_{yz,\,zx}$ states. Similarly, the degenerate O $2p$ orbitals are also split: one can see that the highest VB is primarily composed of O $2p_\pi$ orbitals, instead of O $2p_\sigma$, arising much deeper inside the VB.

The directional dependence of the effective mass (m^*) is shown separately for electron [Fig. 2(a)] and hole [Fig. 2(b)], where m^* is calculated by fitting parabolic functions to the CB and VB edges with particular interest in their anisotropy [28]. Because the (100), (101), and (001) crystalline planes are well known to be the dominant surface facets in TiO_2 particles, carrier transport along directions perpendicular to these three facets, i.e., [100], [1,0,0.15], and [001], respectively, are of particular interest to us. It is important to note that both an electron and a hole exhibit significant anisotropy but in an extremely dissimilar manner. For the electron case, the effective mass is a maximum ($3.70m_0$) in the [001] direction, i.e., z direction, and a minimum ($0.59m_0$) in the [100] or [010] direction, i.e., x or y direction. However, for the hole case, a completely *opposite* trend is observed: the effective mass

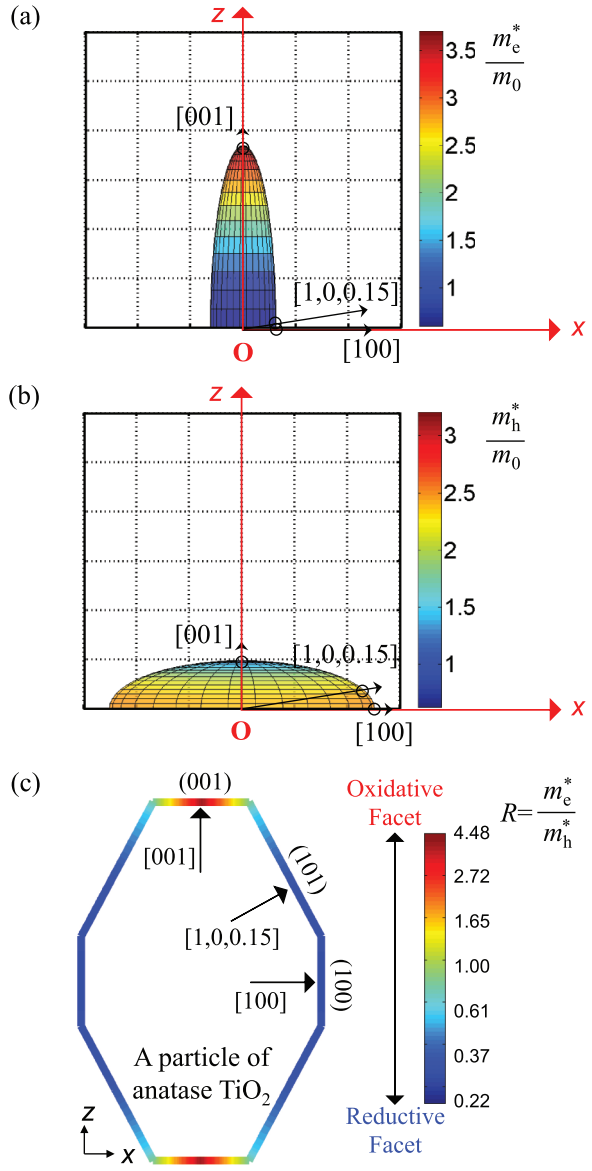

FIG. 2. Anisotropy of electron vs hole effective mass in TiO_2. Circular plots of the (a) electron (m_e^*) and (b) hole (m_h^*) effective mass, as a function of the propagation directions through the lattice on the xz plane. The distance measured from the origin (**O**) to the embedded surface offers relative comparisons of the effective masses between crystal directions. (c) Exemplary schematic of a TiO_2 particle with dominant surface facets. The color code on the facet in indicates the ratio R (m_e^*/m_h^*), which represents the degree of the reductive and oxidative nature of the exposed facets.

is a maximum ($2.33m_0$) in the [100] or [010] direction and a minimum ($0.98m_0$) in the [001] direction. In addition, the effective mass of both electron and hole along the [1,0,0.15] direction [perpendicular to the (101) facet] sits intermediate between the [100] and the [001] cases, but much closer to the [100] side: $m_e^* = 0.61m_0$ and $m_h^* = 2.22m_0$. Parts of these values can be compared to a GW study where effective masses in the [100] direction ($m_e^* = 0.61m_0$ and $m_h^* = 1.90m_0$) are available [29]: results from two approaches are similar.

The aforementioned anisotropy in the effective masses can be related to the photocatalytic activities of facets of TiO_2. Figure 2(c) shows an exemplary schematic of a TiO_2 particle, which resembles those used in previous experiments [13–16,18]. The ratio between the electron and the hole effective mass, defined as $R = m_e^*/m_h^*$, is calculated for an arbitrary crystal direction on the xz plane. Given an inversely proportional relationship between transport mobility and effective mass, R greater than unity ($R > 1$) means that holes can be transported more rapidly than electrons in a specific direction, whereas R less than unity ($R < 1$) means the opposite. It is found that electrons tend to move toward and accumulate on the (100)/(101) facets much more rapidly ($0.26 \leqslant R \ll 1$) than holes do, which makes these two facets much more effective for reduction reactions compared to oxidation reactions. However, for the (001) facet, the opposite would occur: holes would be transported toward the (001) facet much more rapidly than electrons would ($1 \ll R \leqslant 3.95$), resulting in this facet's possessing a highly oxidative nature.

The origin of the effective mass anisotropy can be attributed to orbital hybridizations near the CB and VB edges. To start with the CB side, in Fig. 3(a), the lowest CBs along the [100] vs [001] k direction are shown with a comparison of orbital constitutions (O $2p_\pi$/Ti $3d_{xy}$ ratio). Within the range near the CBM of $|k| \leqslant 0.03$ ($2\pi/$Å), orbital constitutions along the [100] vs [001] direction turn out to be very different: for the [100] direction, O $2p_\pi$/Ti $3d_{xy}$ increases with $|k|$ [8.3% at $|k| = 0.03$ ($2\pi/$Å)], whereas the ratio is constantly 0 for the [001] direction. This is also shown in Figs. 3(b) and 3(c) of the square of wave functions (i.e., partial charge densities) at the selected k points in the CB. In Fig. 3(b), one can see that the contributions of O $2p_\pi$ exist along the [100] k direction: strong d_{xy}-p_π-d_{xy} hybridizations between neighboring Ti and O ions lead to the highly dispersive band. However, in Fig. 3(c), we observe that O $2p_\pi$ orbitals do not emerge at all along the [001] k direction: relatively much weaker d_{xy}-d_{xy} interactions between Ti ions dominate, resulting in the flatlike band.

Let us now move to the VB side: in Fig. 3(d), the highest VBs along the [100] and [001] k directions are compared around the VBM. Unlike the CB side, because the VB primarily consists of O $2p_\pi$ orbitals, we now trace the emergence of Ti $3d$ orbitals along both directions. Interestingly, the ratio Ti $3d$/O $2p_\pi$ remains negligibly low along the [100]; contrary to this, the ratio increases with $|k|$ along [001] [6.7% at $|k| = 0.03$ ($2\pi/$Å)]. These results can visually be confirmed from partial charge density plots at the selected k points in the VB [Figs. 3(e) and 3(f)]. It can be seen that O $2p_\pi$ solely contributes to the VB along the [100] k direction, whereas Ti $3d$ appears along the [001] k direction. As a consequence, unlike the CB case, the VB is more dispersive in the [001] direction, due to the presence of stronger p_π-d-p_π hybridizations between neighboring Ti and O ions than in the [100] case, where relatively much weaker p_π-p_π bonding interactions between O ions dominate.

Thus far, we have investigated the anisotropy of carrier effective masses in pure TiO_2. In photocatalytic applications,

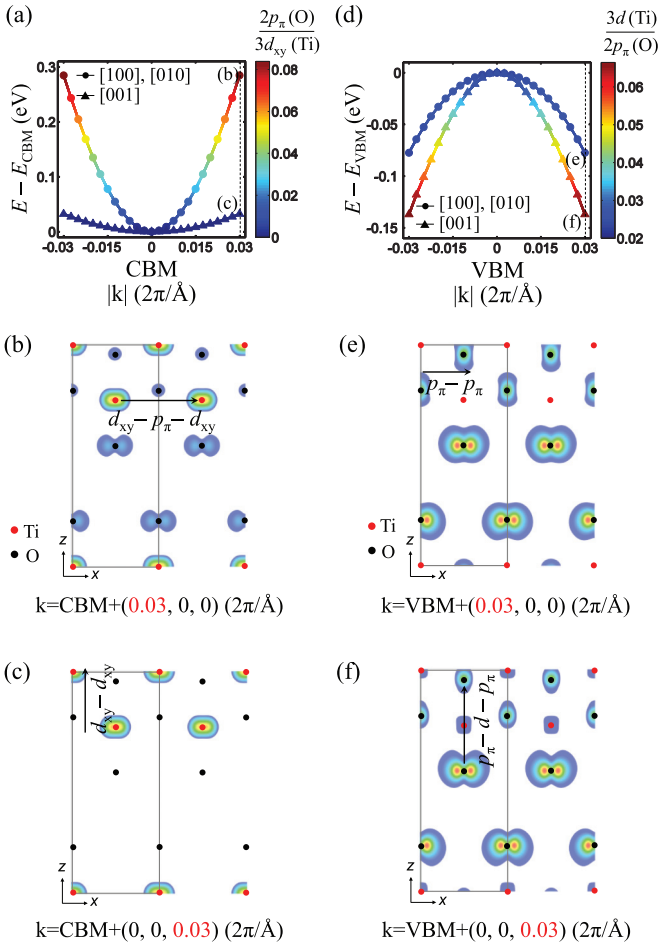

FIG. 3. Origin of opposite anisotropy of electron vs hole effective mass. (a) The lowest CBs along the [100] or [010] (circles) and [001] (triangles) k directions. The color code indicates the ratio O $2p_\pi$/Ti $3d_{xy}$. (b, c) Two-dimensional cross sections of the square of wave functions of the CBs at $k = \text{CBM} + (0.03,0,0)$ $(2\pi/\text{Å})$ (b) and $k = \text{CBM} + (0,0,0.03)$ $(2\pi/\text{Å})$ (c). (d) The highest VBs along the aforementioned directions in (a). The color code indicates the ratio Ti $3d$/O $2p_\pi$. (e, f) The square of wave functions of the VBs at $k = \text{VBM} + (0.03,0,0)$ $(2\pi/\text{Å})$ (e) and $k = \text{VBM} + (0,0,0.03)$ $(2\pi/\text{Å})$ (f). Red and black dots in a unit cell indicate Ti and O atoms in the cross sections, respectively. The isosurface value is 0.002 $e/\text{Å}^3$.

however, in a practical sample, it is likely that a variety of imperfections exist. Thus, to have a broader impact, we expand this study to cases where either dopants or defects are introduced. For doped TiO_2, we selected four transition-metal cation dopants, i.e., W [30], Nb [31], Zr [32], and Y [33], all of which are widely used in PC experiments. These dopants (M) are well known to be incorporated by substituting the Ti ion of the charge state $+q$ (i.e., M_{Ti}^{q+}), rather than being an interstitial: W_{Ti}^{2+}, Nb_{Ti}^{1+}, Zr_{Ti}^{0}, and Y_{Ti}^{1-} [34–36]. For intrinsic defects, we chose the three V_O^{2+}, O_i^{2-}, and Ti_i^{4+}, all of which are well known to be dominant defect types [37–39].

Here, the following key question is of interest to us: *Is the opposite anisotropic behavior of electron vs hole in pure TiO_2 preserved even when either dopants or defects are introduced?* In Fig. 4, we compare the effective mass ratio

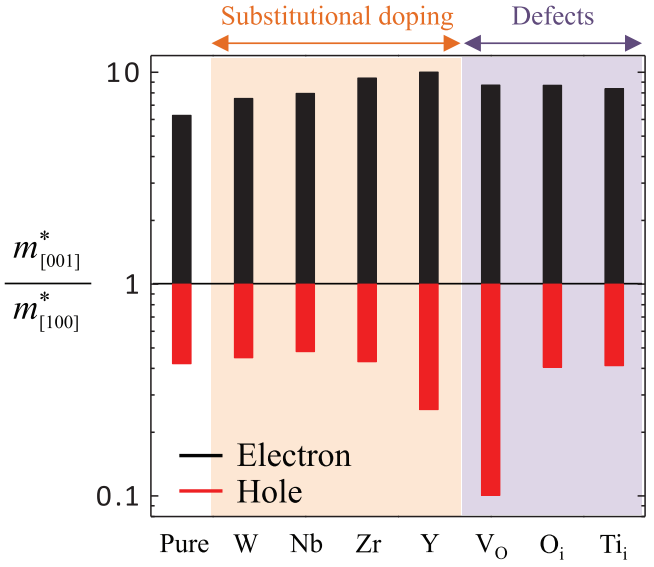

FIG. 4. Comparisons of effective mass anisotropy (log scale) in the presence of dopants and defects.

of the [001] to [100] direction, $m^*_{[001]}/m^*_{[100]}$, of pure TiO_2 and other cases and find that any imperfections introduced in the present study do not change the qualitative trend in the effective mass anisotropy, though they do affect the quantities. For the electron, the ratio $m^*_{[001]}/m^*_{[100]}$ is much larger than unity (7.58–10.04), whereas, for the hole, the ratio is smaller than unity (0.10–0.48), indicating that the opposite trend of anisotropy holds for all cases. The preservation of the trend can be rationalized by the fact that the orbital hybridization does not change much upon the introduction of dopants or defects (see the Supplemental Material [46]).

B. Anisotropy of polaronic transport in TiO_2

It is still under debate whether the dominant carrier transport mechanism is bandlike or polaronic in anatase TiO_2. In Sec. III A, we have assumed that carriers in anatase TiO_2 prefer a delocalized free-carrier state, mainly based on several recent studies [9,40] revealing that polaron formation is rather difficult. However, motivated by polaronic features captured in other studies [41,42], we have performed extensive DFT $+ U$ calculations to investigate the direction dependence of polaron hopping transport (both excess electron and excess hole).

Polaron mobility (μ) in metal oxides is typically modeled within the framework of Marcus/Holstein theory [42–45], where polarons undergo thermally activated hopping from site to site. The formula for the mobility is

$$\mu = \frac{e\mathrm{D}}{k_B\mathrm{T}} = \frac{e(1-c)a^2\nu_0\exp\left(-\frac{\Delta G}{k_B\mathrm{T}}\right)}{k_B\mathrm{T}},$$

where D is the diffusion constant of carriers, $(1-c)$ is the probability that a neighboring site is available for hopping, ΔG is the activation energy for polaron hopping, ν_0 is the optical phonon frequency, k_B is Boltzmann's

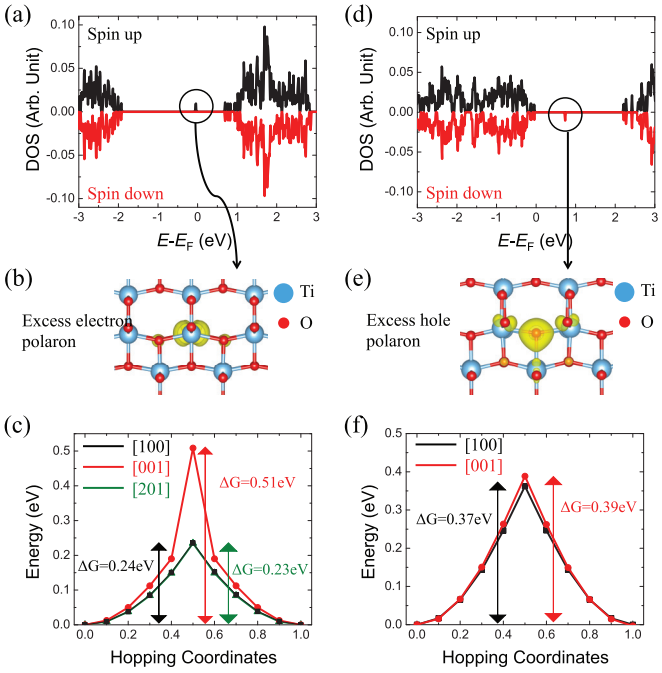

FIG. 5. Direction dependence of polaronic transport of both excess electron (a–c) and excess hole (d–f) in anatase TiO_2. (a) DOS of the extra electron case ($U = 5$ eV). (b) Spin density contour of polaron states (localized on a single Ti atom). (c) Potential energy for polaron hopping along the [100], [001], and [201] directions. (d) DOS of the extra hole case ($U = 5$ eV). (b) Spin density contour of polaron states (localized on a single O atom). (f) Potential energy for polaron hopping along the [100] and [001] directions.

constant, T is the absolute temperature, and a is the hopping distance.

One can see that the mobility (μ) is proportional to $\exp(-\Delta G/k_B T)$. Noting that other factors in the above equation have relatively minor impacts on the mobility, we focus on only ΔG values. The polaron transfer process involves initial, transition, and final states. In the initial state, polaron is mainly localized on a single atom, and in the final state, it is localized on a neighboring atom with the same coordinative environment. In this case, the transition state should occur midway between these two states. The activation energy for polaron hopping (ΔG) can be estimated by calculating the potential energy changes as the polaronic lattice distortions are displaced from the initial to the final geometry. We investigate how ΔG differs by hopping directions of our interests for both electron and hole polarons.

As shown in Figs. 5(a) and 5(b), an excess electron in anatase creates a polaron state within the band gap (lying 0.7 eV below the CBM). This extra electron becomes self-trapped at a Ti site, making itself Ti^{3+} instead of Ti^{4+}. It turns out that each bond between Ti^{3+} and neighboring O anions elongates by 3.09% and 3.72%, respectively, compared to the neutral case. Likewise, as shown in Figs. 5(d) and 5(e), the extra hole creates a polaron state within the band gap (lying 0.8 eV higher than the VBM). This excess hole becomes localized at a selected O site, making itself O^{1-} instead of O^{2-}. Each bond between the O^{1-} anion and neighboring Ti cations increases in length by 0.05%, 0.36%, and 2.16%.

We are particularly interested in their mobility along several directions, which can be indirectly assessed by calculating the activation energies for the hopping (ΔG). For the electron polaron case, we selected three directions, i.e., [100], [001], and [201], as these are (quasi-) perpendicular to three dominant facets of anatase particles, i.e., (100), (001), and (101), respectively. It turns out that ΔG is direction dependent [Fig. 5(c)]: ΔG is similar and small along the [100] and [201] directions ($\Delta G = 0.24$ eV for the [100] direction and $\Delta G = 0.23$ eV for the [201] direction), whereas ΔG is relatively much larger along the [001] direction ($\Delta G = 0.51$ eV). This implies that polarons can hop much faster along the [100] and [201] directions, compared to the [001] direction. Moving on to the excess hole case [Fig. 5(f)], we compared ΔG values of two directions, i.e., [100] and [001]. Unlike the extra electron case, the ΔG values along theses two directions are almost the same: ΔG is 0.37 eV along the [100] direction, and ΔG is 0.39 eV along the [001] direction. In order to check whether this trend is independent of U parameters, we have repeated all calculations at an extreme U value (i.e., $U = 10$ eV). Comparing the results between the $U = 5$ eV and the $U = 10$ eV cases (see the Supplemental Material [46]), we observe that absolute ΔG values increase with the U term, however, their relative order between different directions is preserved in all cases.

Key results are as follows: (i) electrons are transported much more rapidly toward the (100)/(101) facets than the (001), and (ii) almost-isotropic transport is predicted for holes, dissimilarly to the bandlike transport case. It is important to note that, despite the quasi-isotropic hole polaron mobility, our polaron model still supports the preferred accumulations of electrons on the (100)/(101) facets and holes on the (001) facets. This is because the identification of reductive and oxidative facets should be based on the relative order between electron and hole transport mobility. For an example of the (001) facet, ΔG along the [001] direction for an electron (0.51 eV) is much larger than the value for a hole (0.39 eV), which indicates that holes that will survive to the surface will outnumber electrons; as a result, holes would remain on this facet. Likewise, for the (100) facet, ΔG along the [100] direction for an electron (0.24 eV) is much smaller than the value for a hole (0.37 eV), which leads to the conclusion that electrons would remain on this facet. To sum up, despite the isotropic hole polaron mobility, our polaron model also supports the experimental finding, i.e., preferred accumulations of electrons on the (100)/(101) facets and holes on the (001) facets.

IV. CONCLUSION

In summary, using first-principles calculations and assuming bandlike transport, we discover that the anisotropic behavior of electron and hole bulk transport in anatase TiO_2 is the opposite. Meticulous analyses of orbital hybridizations were followed to explain this trend. This finding sheds a new light on the observed reduction/oxidation separations on different facets of TiO_2 particles. For a broader impact, we additionally demonstrate that the opposite trend in anisotropy of electrons vs holes is widely applicable to TiO_2 with dopants or defects. Motivated by the polaronic features in this material,

we expand the study to the case where polaron hopping is the dominant transport mechanism. Our polaron model also predicts dissimilar anisotropic behavior of electron vs hole bulk transport and supports the observed facet dependence of the photochemical activity of anatase TiO_2.

ACKNOWLEDGMENTS

This work was supported by the Creative Materials Discovery Program through the National Research Foundation of Korea (NRF-2016M3D1A1021140) and KIST institutional project (No. 2E26130). The authors thank KISTI for providing computational resources (Project No. KSC-2015-C2-033).

[1] X. Chen and S. S. Mao, Chem. Rev. **107**, 2891 (2007).

[2] R. Wang, K. Hashimoto, A. Fujishima, M. Chikuni, E. Kojima, A. Kitamura, M. Shimohigoshi, and T. Watanabe, Nature **388**, 431 (1997).

[3] A. Fujishima and K. Honda, Nature **238**, 37 (1972).

[4] J. Schneider, M. Matsuoka, M. Takeuchi, J. Zhang, Y. Horiuchi, M. Anpo, and D. W. Bahnemann, Chem. Rev. **114**, 9919 (2014).

[5] S. Wendt, J. Matthiesen, R. Schaub, E. K. Vestergaard, E. Laegsgaard, F. Besenbacher, and B. Hammer, Phys. Rev. Lett. **96**, 066107 (2006).

[6] G. H. Enevoldsen, H. P. Pinto, A. S. Foster, M. C. R. Jensen, W. A. Hofer, B. Hammer, J. V. Lauritsen, and F. Besenbacher, Phys. Rev. Lett. **102**, 136103 (2009).

[7] M. Xu, Y. Gao, E. M. Moreno, M. Kunst, M. Muhler, Y. Wang, H. Idriss, and C. Wöll, Phys. Rev. Lett. **106**, 138302 (2011).

[8] J. Zhang, P. Zhou, J. Liu, and J. Yu, Phys. Chem. Chem. Phys. **16**, 20382 (2014).

[9] M. Setvin, C. Franchini, X. Hao, M. Schmid, A. Janotti, M. Kaltak, C. G. Van de Walle, G. Kresse, and U. Diebold, Phys. Rev. Lett. **113**, 086402 (2014).

[10] G. Liu, H. G. Yang, J. Pan, Y. Q. Yang, G. Q. Lu, and H.-M. Cheng, Chem. Rev. **114**, 9559 (2014).

[11] H. G. Yang, C. H. Sun, S. Z. Qiao, J. Zou, G. Liu, S. C. Smith, H. M. Cheng *et al.*, Nature **453**, 638 (2008).

[12] X. Han, Q. Kuang, M. Jin, Z. Xie, and L. Zheng, J. Am. Chem. Soc. **131**, 3152 (2009).

[13] J. Pan, G. Liu, G. Q. Lu, and H.-M. Cheng, Angew. Chem. Int. Ed. **50**, 2133 (2011).

[14] T. Tachikawa, S. Yamashita, and T. Majima, J. Am. Chem. Soc. **133**, 7197 (2011).

[15] X. Wang, R.-G. Li, Q. Xu, H.-X. Han, and C. Li, Acta Phys.-Chim. Sin **29**, 1566 (2013).

[16] N. Roy, Y. Sohn, and D. Pradhan, ACS Nano **7**, 2532 (2013).

[17] C. Li, C. Koenigsmann, W. Ding, B. Rudshteyn, K. R. Yang, K. P. Regan, S. J. Konezny, V. S. Batista, G. W. Brudvig *et al.*, J. Am. Chem. Soc. **137**, 1520 (2015).

[18] A. Selloni, Nat. Mater. **7**, 613 (2008).

[19] J. Yu, J. Low, W. Xiao, P. Zhou, and M. Jaroniec, J. Am. Chem. Soc. **136**, 8839 (2014).

[20] Z. Zheng, B. Huang, J. Lu, X. Qin, X. Zhang, and Y. Dai, Chem. Eur. J. **17**, 15032 (2011).

[21] J. Li, L. Cai, J. Shang, Y. Yu, and L. Zhang, Adv. Mater. **28**, 4059 (2016).

[22] G. Kresse and J. Furthmuller, Comput. Mater. Sci. **6**, 15 (1996).

[23] G. Kresse and D. Joubert, Phys. Rev. B **59**, 1758 (1999).

[24] J. Ihm, A. Zunger, and M. L. Cohen, J. Phys. C: Solid State Phys. **12**, 4409 (1979).

[25] J. Heyd, G. E. Scuseria, and M. Ernzerhof, J. Chem. Phys. **124**, 219906 (2006).

[26] M. Horn, C. F. Schwerdtfeger, and E. P. Meagher, Z. Kristallogr. **136**, 273 (1972).

[27] R. Asahi, Y. Taga, W. Mannstadt, and A. J. Freeman, Phys. Rev. B **61**, 7459 (2000).

[28] Effective mass is calculated according to

$$m^* = \pm\hbar^2\left(\frac{d^2E}{dk^2}\right)^{-1},$$

where $\hbar$ is the reduced Planck constant, and E is the band energy as a function of the wave vector k. The fitting range is $|k| < 0.1$ Å^{-1}.

[29] L. Thulin and J. Guerra, Phys. Rev. B **77**, 195112 (2008).

[30] H. Choi, D. Shin, B. C. Yeo, T. Song, S. S. Han, N. Park, and S. Kim, ACS Catal. **6**, 2745 (2016).

[31] Y. Gai, J. Li, S.-S. Li, J.-B. Xia, and S.-H. Wei, Phys. Rev. Lett. **102**, 036402 (2009).

[32] B. Gao, T. M. Lim, D. P. Subagio, and T.-T. Lim, Appl. Catal. A Gen. **375**, 107 (2010).

[33] M. Khan and W. Cao, J. Mol. Catal. A Chem. **376**, 71 (2013).

[34] H. Kamisaka, T. Hitosugi, T. Suenaga, T. Hasegawa, and K. Yamashita, J. Chem. Phys. **131**, 034702 (2009).

[35] M. Sacerdoti, M. C. Dalconi, M. C. Carotta, B. Cavicchi, M. Ferroni, S. Colonna, and M. L. D. Vona, J. Solid State Chem. **177**, 1781 (2004).

[36] S. X. Zhang, D. C. Kundaliya, W. Yu, S. Dhar, S. Y. Young, L. G. Salamanca-Riba, S. B. Ogale, R. D. Vispute *et al.*, J. Appl. Phys. **102**, 013701 (2007).

[37] X. Chen, L. Liu, and F. Huang, Chem. Soc. Rev. **44**, 1861 (2015).

[38] A. Janotti, J. B. Varley, P. Rinke, N. Umezawa, G. Kresse, and C. G. Van de Walle, Phys. Rev. B **81**, 085212 (2010).

[39] G. Mattioli, P. Alippi, F. Filippone, R. Caminiti, and A. A. Bonapasta, J. Phys. Chem. C **114**, 21694 (2010).

[40] C. Spreafico and J. Van de Vondele, Phys. Chem. Chem. Phys. **16**, 26144 (2014).

[41] C. D. Valentin and A. Selloni, J. Phys. Chem. Lett. **2**, 2223 (2011).

[42] N. A. Deskins and M. Dupuis, Phys. Rev. B **75**, 195212 (2007).

[43] N. A. Deskins and M. Dupuis, J. Phys. Chem. C **113**, 346 (2009).

[44] T. Liu, X. Zhou, M. Dupuis and C. Li, Phys. Chem. Chem. Phys. **17**, 23503 (2015).

[45] A. Janotti, C. Franchini, J. B. Varley, G. Kresse, and C. G. Van de Walle, Phys. Status Solidi RRL **7**, 199 (2013).

[46] See Supplemental Material at http://link.aps.org/supplemental/10.1103/PhysRevB.95.045209 for functional dependence of effective masses, partial charge densities for the cases of dopants and defects, and U-parameter dependence of the polaronic transport.